

The Effects of Accelerated Photooxidation on Molecular Weight and Thermal and Mechanical Properties of PHBV/Cloisite 30B Bionanocomposites

Kahina Iggui^{1,2,*}, Mustapha Kaci², Nicolas Le Moigne¹ and Anne Bergeret¹

¹Centre des Matériaux des Mines d'Alès (C2MA), IMT Mines Ales, Université de Montpellier, 30100 Alès, France

²Laboratory of Advanced Polymer Materials, University of Béjaïa, Béjaïa Province, 06000, Algeria

^{*}Current address: Institut de Technologie, Université Akli Mohand Oulhadj, Bouira 10000, Algeria

[†]C2MA is member of the European Polysaccharide Network of Excellence (EPNOE)

Received May 31, 2017; Accepted November 11, 2017

ABSTRACT: The effects of accelerated photooxidation on the molecular weight and thermal and mechanical properties of Cast PHBV and PHBV/Cloisite 30B (3 wt%) bionanocomposites are investigated herein. Through size exclusion chromatography (SEC) analysis, a significant decrease in both weight and number average molecular weights was observed for all irradiated samples over time, resulting from the chain scission mechanism. Differential scanning calorimetry (DSC) data indicated a decrease in degree of crystallinity and melting temperature after UV exposure, with the appearance of double melting peaks related to the changes in the crystal structure of PHBV. Thermal stability, tensile and thermo-mechanical properties were also reduced consecutively in photooxidation, being more pronounced for Cast PHBV. This study shows that the incorporation of Cloisite 30B in PHBV provides a better resistance to photooxidation in comparison with the neat polymer.

KEYWORDS: Poly(3-hydroxybutyrate-co-3-hydroxyvalerate), organo-modified montmorillonite, bionanocomposites, accelerated photooxidation and degradation

1 INTRODUCTION

In recent years, much attention has been focused on the study of stabilization of bionanocomposite materials in order to predict their lifetime and behavior in outdoor applications [1–3]. Indeed, polymers may degrade when exposed to environmental factors, such as temperature, humidity, UV light exposure and so on, which affect their overall performances [4–5]. In order to determine the aging mechanisms of polymeric materials under service conditions, two types of environmental aging tests have been developed: natural aging tests under outdoor exposure conditions and artificial aging tests reproducing natural aging under accelerated conditions with laboratory equipments [6–8].

To minimize environmental pollution, conventional plastics can potentially be replaced with biodegradable polymers that can be produced from renewable

resources [9–10]. Among the biodegradable polymers, poly(hydroxyalkanoates) (or PHAs), including poly(3-hydroxybutyrate) (PHB) and poly(3-hydroxybutyrate-co-3-hydroxyvalerate) (PHBV), are among the most studied ones [11–12]. Most of the degradation studies on PHAs have been focused on thermal degradation [13–14], and biodegradation behavior of PHB and PHBV in water [15], soil [16–18], waste compost [19–20], and enzymes [21, 22]. However, only a few studies have been conducted on photooxidation of PHAs. In this regard, the effect of accelerated weathering exposure on PHBV was studied by Wei and McDonald [23]. The film samples were exposed to a repeated 2 h cycle of UV radiation followed by 2 h of combined UV radiation and water spray. The authors proposed five types of degradation mechanisms that can take place during PHBV weathering: (1) Norrish Type I, (2) Norrish Type II, (3) radical initiation, (4) crosslinking reaction, and (5) some extent of hydrolysis of ester bonds, primarily resulting in a decrease in molecular weight. The effect of UVA radiation on PHB was investigated by Sadi *et al.* [24]. The results showed that PHB undergoes both chain scission and crosslinking reactions and

*Corresponding author: iguikahina@yahoo.fr

the formation of carbonyl groups was detected. These changes in the chemical structure of PHB resulted in the appearance of cracks and whitening of the PHB samples surfaces, accompanied by a decrease in the melting temperature and mechanical properties, and substantial increase in the degree of crystallinity. The authors also argued that Norrish II reaction probably did not take place in the case of PHB photooxidation. Furthermore, accelerated weathering conditions with cyclic humidity and ultraviolet (UV) light exposure on PHB films and PHB/hemp-fiber reinforced composites were investigated by Michel and Billington [25]. Two distinct weathering procedures were performed, one with cyclic elevated relative humidity and one at constant humidity. The authors reported that neat PHB polymer films exhibit increased elastic modulus and decreased ultimate strength and strain with increasing weathering exposure time, while PHB/hemp-fiber composites exhibit decreased ultimate strength and elastic modulus after exposure, attributed to combined cyclic fiber swelling and embrittlement of the biopolymer matrix through photooxidation and hydrolysis. Both neat PHB and PHB/hemp-fiber composites experienced mass loss and increased fading upon weathering exposure. Moreover, degradation rates of polymer matrices can be influenced by the presence of layered silicate nanoclays, such as montmorillonite (MMT), often used to enhance some of their properties. Indeed, several authors have found a catalytic effect of montmorillonite on hydrolytic degradation and biodegradation of different aliphatic polyesters, due to the high hydrophilicity of these nanoparticles [26–28]. Furthermore, significant degradation could also be induced by the presence of Al Lewis acid sites in the inorganic layers of montmorillonite which catalyzes the hydrolysis of ester linkages of polyesters [29–30], and the decomposition of the organo-modifiers upon extrusion that could also catalyze degradation [31–32]. However, other authors have reported that nanoclays may retard the degradation of aliphatic polyesters due to the enhanced barrier properties of the layered silicate nanocomposites [33–35]. Among the tremendous amount of literature devoted to aging of nanocomposite materials, the behavior of PHBV-based bionanocomposites under ultraviolet (UV) photooxidation has not yet been reported.

Therefore, the objective of this work was to investigate the effects of accelerated photooxidation on the molecular weight and thermal and mechanical properties of PHBV/Cloisite 30B (3 wt%) bionanocomposite with respect to neat PHBV. The material changes induced by the accelerated photooxidation were evaluated by several techniques, including size exclusion chromatography (SEC), differential scanning calorimetry (DSC), thermogravimetric analysis (TGA),

dynamic mechanical analysis (DMA), tensile testing and scanning electron microscopy (SEM).

2 EXPERIMENTAL

2.1 Materials and Preparation of PHBV/C30B Nanocomposite Films

Poly(3-hydroxybutyrate-co-3-hydroxyvalerate) (PHBV) was supplied by NaturePlast (France) under the trade name PHI 002[®] with 7 wt% of hydroxyvalerate (HV). It is nucleated with boron nitride and used as received. It is a semicrystalline polymer with a glass transition temperature of around 5 °C and a melting temperature of around 155 °C according to the supplier data sheet.

The nanoclay used was supplied by Southern Clay Products, Inc. (USA) under the trade name Cloisite 30B[®], named C30B. According to the manufacturer, it was organically modified by bis-(2-hydroxyethyl) methyl tallow alkyl ammonium cations with 65% C18, 30% C16 and 5% C14 and cation exchange capacity of 90 meq/100 g. PHBV matrix and C30B clays were dried under vacuum overnight at 80 °C before use.

The bionanocomposite sheet samples, named C-PHBV/3C30B, prepared at a filler content of 3 wt%, were produced by masterbatch dilution with neat PHBV using a single-screw cast extruder, as detailed in a previous paper [20]. The sheets obtained, having an average thickness of about 500 µm and 80 mm width, were then stored at 20 °C and 2% RH. Our previous study [20] demonstrated through STEM observations, WAXD measurements and thermo-mechanical analyses the formation of intercalated bionanocomposites, with a few individually dispersed platelets attesting to a partial exfoliation of MMT.

2.2 Accelerated Photooxidation Conditions

The sheet samples of both Cast PHBV and C-PHBV/3C30B (3 wt%) bionanocomposites were subjected to accelerated UV exposure up to 4500 h using a SEPAP 12/24 photo-aging chamber, which is equipped with four mercury-vapor arc lamps. The power of each lamp is 400 watts and the temperature in the chamber is fixed at 63 °C due to the lamps' emission. The specimens, in the shape of an ISO ½ dumbbell, were placed in their sample holders on a cylindrical turret and a regular circular rotation was applied upon UV exposure to ensure uniform aging. The samples were collected periodically for testing between 0 to 4500 hours.

2.3 Characterization Methods

2.3.1 Size-Exclusion Chromatography (SEC)

The molecular weight changes of neat PHBV samples and their bionanocomposites before and after accelerated UV aging were determined by size-exclusion chromatography (SEC) using an Omni-SECT 60A system. Samples of Cast PHBV and C-PHBV/3C30B bionanocomposites (typically 20 mg) were dissolved in 2 ml of chloroform over 1 h at 60 °C. Before injection, all samples were filtered through a Phenex PTFE 0.2 mm filter to remove any insoluble fractions or clays. SEC experiments were conducted in a Waters 410 differential refractometer using a PL Gel 5-mm Mixed-C column (1 × 600 mm). The column eluent was chloroform at a flow rate of 1 mL/min and polystyrene standards were used for calibration. The average molecular weights in weight \bar{M}_w and in number \bar{M}_n well as the polydispersity index (\mathcal{D}) were determined. Two specimens of each sample were tested.

2.3.2 Differential Scanning Calorimetry (DSC)

Differential scanning calorimetry analysis was performed on a Pyris Diamond DSC thermal analysis system (PerkinElmer) equipped with an IntraCooler II. Small amounts (15 to 20 mg) of dried samples were placed into aluminum pans. Heating and cooling scans were performed at a scanning rate of 10 °C min⁻¹ from 30 to 200 °C, using N₂ as the purging gas. At least three specimens were tested for each sample. An empty aluminum pan was used as reference and the crystallization exotherm and melting endotherm were analyzed. The degree of crystallinity (X_c) was determined according to Equation 1:

$$X_c = \frac{\Delta H_m}{W \cdot \Delta H_m^0} \times 100 \quad (1)$$

where ΔH_m (J.g⁻¹) is the melting enthalpy of the polymer matrix PHBV, W is polymer weight fraction (PHBV) in the sample, calculated from the real content of C30B, and ΔH_m^0 is the melting enthalpy of a pure crystal and $\Delta H_m^0 = 146$ J.g⁻¹ [36].

2.3.3 Thermogravimetric Analysis (TGA)

Thermogravimetric analysis measurements were carried out using a Pyris Diamond thermogravimetric analyzer (PerkinElmer) on specimens of 10–12 mg at a heating rate of 10 °C/min. Samples were heated from room temperature up to 700 °C to reach the complete thermal degradation of PHBV and its bionanocomposites. All tests were performed under nitrogen atmosphere.

2.3.4 Dynamic Mechanical Analysis (DMA)

The thermo-mechanical behavior of Cast PHBV and C-PHBV/3C30B bionanocomposite samples was investigated in the vicinity of the α -transition using a DMA 50 dynamic mechanical analyzer (Metravib O3dB, France). Three rectangular specimens of each sample with dimensions of approximately 35 × 5 × 0.5 mm³ were tested. The measurements were performed in shear mode at 5 Hz and 5 mm of amplitude and the temperature range was varied between 20 and 120 °C at a heating rate of 3 °C/min. Storage modulus (G'), loss modulus (G'') and loss factor ($\tan \delta$) were determined.

2.3.5 Tensile Testing

The mechanical properties were measured with a universal testing machine (Zwick/Roell) at room temperature according to ASTM standard method (ISO 527). The extension was set at 1 mm/min, using an incremental clip-on extensometer (Zwick/Roell). Five specimens were tested for each material and the average value was calculated for Young's modulus, tensile strength and elongation at break.

2.3.6 Scanning Electron Microscopy (SEM)

The SEM images of Cast PHBV and C-PHBV/3C30B bionanocomposite films were captured using a Quanta 200 FEG (FEI Company) environmental scanning electron microscope at an acceleration voltage of 7 to 10 keV. Prior to observations in scanning mode (SEM), the fracture surfaces of the films in liquid nitrogen were sputter-coated with carbon using a CED 030 carbon evaporator device (Balzers) to ensure good surface conductivity and avoid degradation under electron beam upon observation.

3 RESULTS AND DISCUSSION

3.1 Molecular Weight Changes

Table 1 reports the values of the weight average molecular weight \bar{M}_w , number average molecular weight \bar{M}_n and polydispersity index (\mathcal{D}) for Cast PHBV and C-PHBV/3C30B bionanocomposite samples after 880 and 4500 h of exposure under accelerated UV conditions. A significant reduction can be noticed in the average molecular weight for both materials. Indeed, upon increasing exposure time to 4500 h, PHBV exhibits a decrease in both \bar{M}_w and \bar{M}_n by almost 65% and 86.5%, respectively. The same trend is also observed for \bar{M}_w and \bar{M}_n of C-PHBV/3C30B bionanocomposite samples,

Table 1 Weight-average molecular weight \overline{M}_w , number-average molecular weight \overline{M}_n and polydispersity index (\mathfrak{D}) of Cast PHBV and C-PHBV/3C30B bionanocomposites as a function of exposure time.

Samples	Exposure time (h)	\overline{M}_w (g / mol)	\overline{M}_n (g / mol)	\mathfrak{D}
Cast PHBV	0	290860 ± 2881	112950 ± 12632	2.6 ± 0.26
	880	178220 ± 9326	52920 ± 2896	2.4 ± 0.01
	4500	103080 ± 15216	15200 ± 1913	6.8 ± 0.15
C- PHBV/3C30B	0	305510 ± 1971	94640 ± 5460	3.2 ± 0.17
	880	186450 ± 5728	47160 ± 12745	4.1 ± 0.98
	4500	113590 ± 3837	21480 ± 9248	5.4 ± 0.50

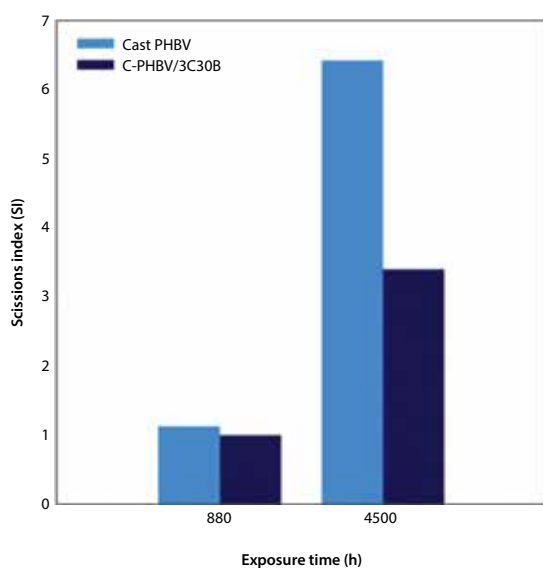
showing a decrease in \overline{M}_w and \overline{M}_n by about 63% and 77%, respectively. According to the literature [37–38], the decrease of the average molecular weight associated with an enhanced polydispersity for both Cast PHBV and C-PHBV/3C30B during the accelerated photooxidation process is explained as a result of degradation, which primarily takes place in the amorphous regions of the polymer matrix via chain scission mechanism. Indeed, Wei *et al.* [23] and Sadi *et al.* [24] reported that the chain scission mechanism likely occurs via Norrish reaction and radical initiation mechanisms. These results are in good agreement with those presented in Figure 1, indicating the chain scission index (SI) values for each sample with increased exposure time, determined according to Equation 2:

$$SI = \left[\frac{\overline{M}_n(t_0)}{\overline{M}_n(t)} \right] - 1 \quad (2)$$

where $\overline{M}_n(t_0)$ and $\overline{M}_n(t)$ are the initial number average molecular weight and the number average molecular weight at a given exposure time, respectively. Figure 1 shows a significant increase in the SI value for Cast PHBV and C-PHBV/3C30B bionanocomposite samples from 1.13 to 6.42 and from 1 to 3.40, respectively, at 880 and 4500 h. These results clearly indicate the occurrence of chain scission in the irradiated samples. Furthermore, it is worth mentioning that the extent of chain scission was less pronounced for PHBV/C30B bionanocomposite.

3.2 Thermal Properties

Figure 2 shows the DSC thermograms recorded during the second heating scans for Cast PHBV and C-PHBV/3C30B samples at different exposure times. The DSC data are reported in Table 2. For all irradiated samples, a decrease in the melting temperature (T_m) is observed with increased exposure time. Furthermore, the DSC thermograms of the irradiated samples exposed up to 2000 h exhibit double melting peaks, exhibiting a main peak T_{m1} at 165 and 167 °C and a secondary peak T_{m2} at lower temperature, i.e., 156 and 162 °C, for Cast PHBV and bionanocomposites C-PHBV/3C30B, respectively. The appearance of a shoulder corresponding to a third melting peak T_{m3} for the bionanocomposite sample above 2000 h of UV exposure is also observed. The third peak decreases from 155 °C to 152 °C with time. The literature [39–41] attributed the formation of secondary melting peaks to changes in the chemical structure and organization of the polymer chains during UV irradiation that leads to the formation of crystal populations with different

**Figure 1** Chain scission index (SI) of Cast PHBV and C-PHBV/3C30B bionanocomposite films.

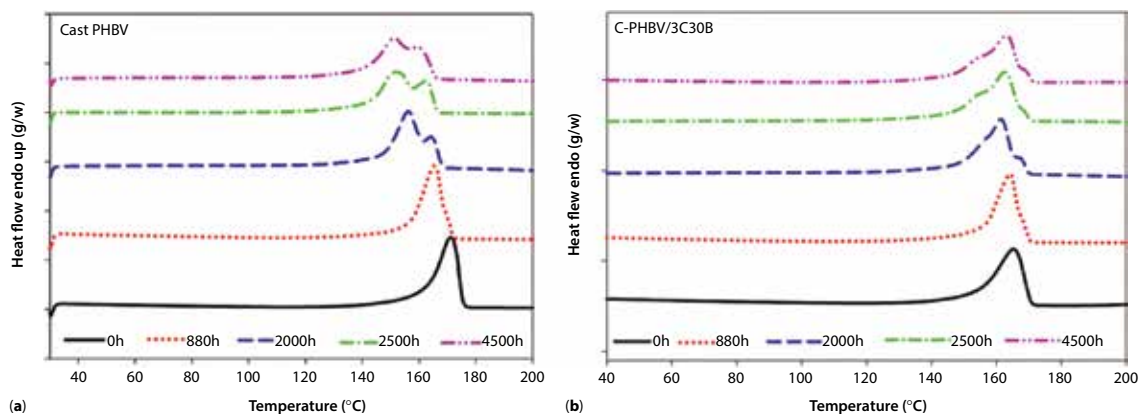


Figure 2 DSC thermograms of (a) Cast PHBV and (b) C-PHBV/3C30B bionanocomposites during second heating scans at different exposure times.

Table 2 Thermal characteristics (crystallization temperature T_c , melting temperature T_m and crystalline index X_c) obtained from the cooling and the second heating of Cast PHBV and C-PHBV/3C30B Bionanocomposites as a function of exposure time.

Samples	Exposure time (h)	T_c (°C)	T_{m3} (°C)	T_{m2} (°C)	T_{m1}	X_c (%)
Cast PHBV	0	119 ± 0.5	–	–	170 ± 0.5	66.1 ± 1
	880	115 ± 2	–	–	165 ± 0.5	64.6 ± 0.5
	1500	114 ± 1.5	–	–	165 ± 0.5	62.8 ± 1
	2000	114 ± 0.5	–	156 ± 0.5	165 ± 0.5	64.5 ± 0.5
	2500	110 ± 1.5	–	152 ± 1	162 ± 0.5	62.5 ± 2
	4500	112 ± 1	–	152 ± 1	159 ± 0.5	62.5 ± 1
C-PHBV/3C30B	0	119 ± 0.5	–	–	165 ± 0.5	63.4 ± 0.5
	880	114 ± 0.5	–	–	164 ± 0.5	63.9 ± 0.5
	1500	115 ± 0.5	–	–	165 ± 0.5	62.3 ± 0.5
	2000	116 ± 1	155 ± 0.5	162 ± 0.5	167 ± 0.5	63.4 ± 1
	2500	115 ± 0.5	154 ± 0.5	155 ± 0.5	163 ± 0.5	63.9 ± 0.5
	4500	116 ± 0.5	152 ± 0.5	154 ± 0.5	163 ± 0.5	62.5 ± 0.5

perfections and lamellar thicknesses. Moreover, the overall decrease in melting temperature with exposure time may also be attributed to the significant decrease in molecular weight of polymer chains [42–43]. Figure 3 shows the relationships between the crystallization temperature (T_c), the crystallinity index (X_c) and the exposure time for Cast PHBV and C-PHBV/3C30B samples. A slight decrease of T_c and X_c is observed with increasing exposure time. The decrease of T_c is attributed to chain scission mechanism, which promotes the formation of shorter macromolecular chains with higher mobility. Therefore, short chains have the ability to orient themselves into an ordered structure intramolecularly or intermolecularly at a lower temperature compared to long molecular chains [41,

44]. On the other hand, the decrease of X_c may result from the damage of the crystallites by UV irradiation, which promotes imperfections in crystalline structure [39–41, 45].

Additional data about changes in thermal stability induced by accelerated photooxidation exposure of Cast PHBV and C-PHBV/3C30B bionanocomposite samples were obtained by TGA analysis. The degradation temperature values at 5% and 50% weight loss and the maximum degradation rate, in addition to the char percentage at 600 °C, are summarized in Table 3. The TGA and DTG thermograms for C-PHBV/3C30B bionanocomposites as a function of exposure time taken as an example are shown in Figure 4. Before exposure to accelerated UV testing, C-PHBV/3C30B

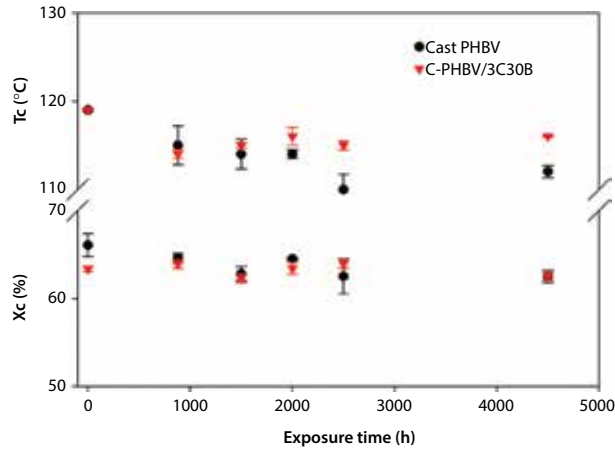


Figure 3 T_c and X_c changes of Cast PHBV and C-PHBV/3C30B samples with exposure time (0–4500 h).

bionanocomposite sample exhibits the higher thermal stability (+8 °C) compared to Cast PHBV. This is due to the presence of the organoclay, which reduces the diffusion of the volatile degradation products of the bionanocomposite sample [37–38]. After UV irradiation, a decrease in the degradation temperature values is observed for both PHBV and its bionanocomposite with increasing exposure time, probably due to the reduction of the molecular weight of samples arising as photolysis products that could catalyze degradation of polymer [38, 46–47]. For Cast PHBV $T_{5\%} = 263 \pm 1$ °C is decreased by 11 °C after 4500 h of exposure. This effect is more pronounced when PHBV contains 3 wt% of Cloisite 30B, indicating a faster thermal degradation. $T_{5\%}$ also shifts to lower values, reducing from 266 ± 1 °C to 244 ± 1 °C after 4500 h of exposure, representing a decrease of 22 °C. A similar trend is observed with the

Table 3 The decomposition temperatures at 5%, 50% weight loss, the maximum degradation rate and the char residue at 600 °C of Cast PHBV and C-PHBV/3C30B bionanocomposites as a function of exposure time.

Samples	Exposure time (h)	$T_5\%$ (°C)	$T_{50\%}$ (°C)	$T_{\text{max. rate}} T_{\text{vmd}}$ (°C)	Char (%) at 600(°C)
Cast PHBV	0	263	282	285	1.3
	880	260	282	284	1.4
	1500	258	279	283	1.7
	2500	254	276	280	1.5
	4500	252	275	278	1.5
C-PHBV/3C30B	0	266	290	293	3.6
	880	260	288	293	4.2
	1500	-	-	-	-
	2500	263	270	286	3.5
	4500	244	277	286	4.1

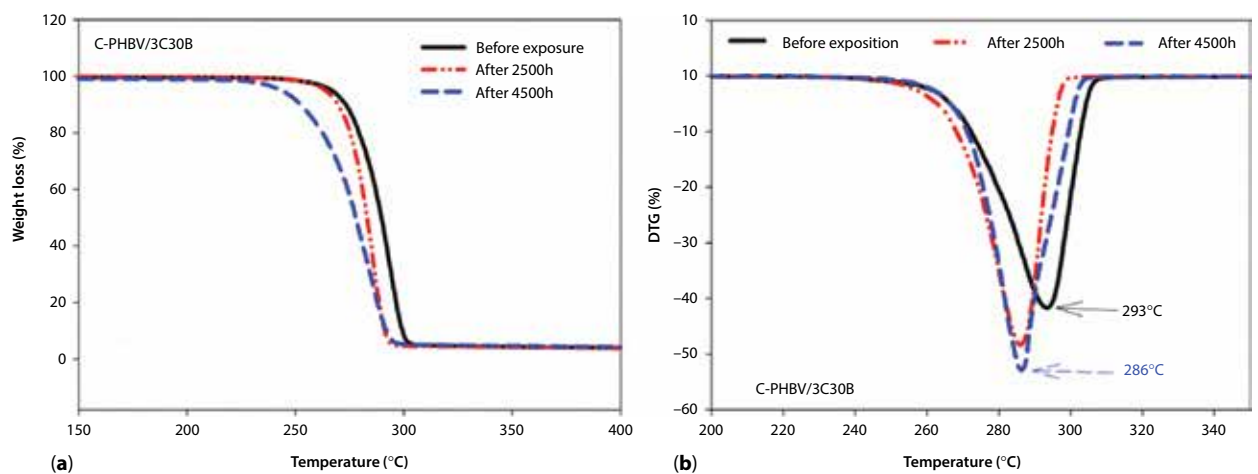


Figure 4 (a) TGA and (b) DTG curves of C-PHBV/3C30B bionanocomposites before exposure and after 2500 and 4500 hours exposure to accelerated photooxidation.

degradation temperature at 50% weight loss for both Cast PHBV and C-PHBV/3C30B bionanocomposite samples. However, before accelerated photooxidation exposure, the decomposition temperatures at the maximum degradation rate (T_{vmd}) of C-PHBV/3C30B bionanocomposites increased compared to Cast PHBV, indicating the enhancement of thermal stability with the incorporation of C30B. After exposure, there is no significant change in the maximum degradation rate of C-PHBV/3C30B bionanocomposites even after 4500 h compared to that of Cast PHBV. The values of the decomposition temperature at the maximum degradation rate (T_{vmd}) of C-PHBV/3C30B decreases from 293 °C to reach the value of the non-irradiated Cast PHBV observed at 285 °C. These results indicate a lower degradation rate at given temperature for the bionanocomposite sample, which could be attributed to the protective role of C30B nanoclays acting as an insulating barrier.

3.3 Thermo-Mechanical Properties

Figure 5 shows the curves of storage modulus (G') for Cast PHBV and C-PHBV/3C30B bionanocomposite samples before and at exposure time of 880, 2000 and 2500 hours. The results indicate that before UV irradiation, an enhancement of storage modulus (G') is clearly observed for the bionanocomposite sample compared to PHBV. This may be related to the high stiffness of clays, their good dispersion and the good interactions occurring between the PHBV matrix and C30B that should restrict the polymer chains mobility [20]. Under accelerated photooxidation, it is noted that the storage modulus is significantly reduced for both Cast PHBV and C-PHBV/3C30B bionanocomposite samples with increasing irradiation time. This phenomenon is explained as a result of the reduction

in molecular weights of PHBV (Table 1) due to chain scission, which greatly alters the thermo-mechanical properties of the PHBV matrix. The addition of 3 wt% of C30B seems to have no positive effect on the thermo-mechanical stability of PHBV when exposed to UV aging. Indeed, the drop in storage modulus is almost similar to that of cast PHBV and no shift in the alpha transition is observed.

3.4 Tensile Properties

The variations in Young's modulus, tensile strength and elongation at break for both Cast PHBV and C-PHBV/3C30B bionanocomposite samples are presented in Figure 6 as a function of exposure time. The values are also summarized in Table 4. For Cast PHBV, it is observed that the values of Young's modulus remain fairly constant up to 880 h before decreasing gradually with exposure time. Indeed, at 4500 h, the Young's modulus value decreases by 23% as compared to non-irradiated PHBV. This could be due to the significant reduction in molecular weight resulting from the chain scission mechanism. Similar data were reported by Gorrasi *et al.* [48] for PLA after 300 h of exposure in a UV climatic chamber at 30°C and 50% RH. Moreover, tensile strength and elongation at break both decrease drastically with exposure time, to reach a maximum loss of 67% and 45% at 4500 h, respectively. In this regard, Sadi *et al.* [24] and Wei and McDonald [23] reported a reduction in tensile strength and elongation at break by 58% and 46% for PHB and PHBV subjected to accelerated photooxidation, respectively. A lower decrease in the mechanical properties was observed for the C-PHBV/3C30B bionanocomposite samples compared to the Cast PHBV along the photooxidation process. Indeed, after 4500 h of exposure to accelerated UV irradiation, Young's modulus,

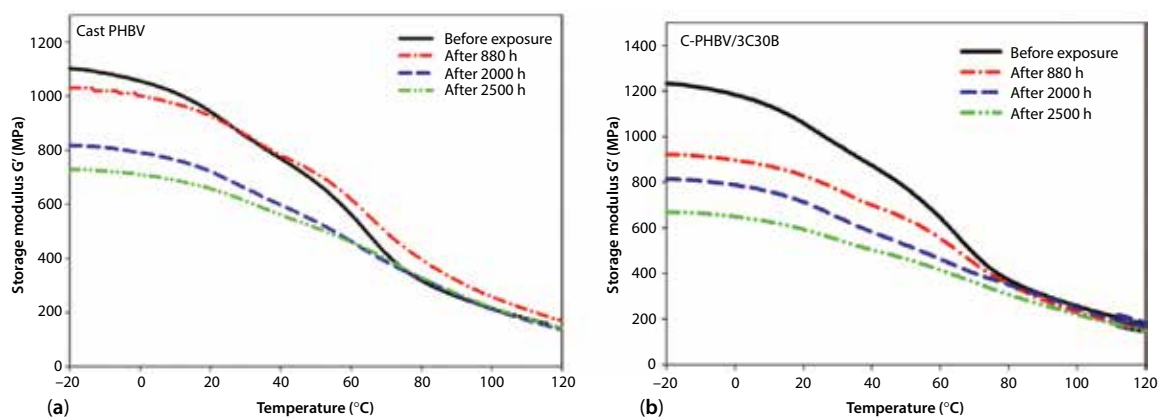


Figure 5 Temperature dependence of storage modulus (G') for (a) Cast PHBV and (b) C-PHBV/3C30B bionanocomposites as a function of exposure time.

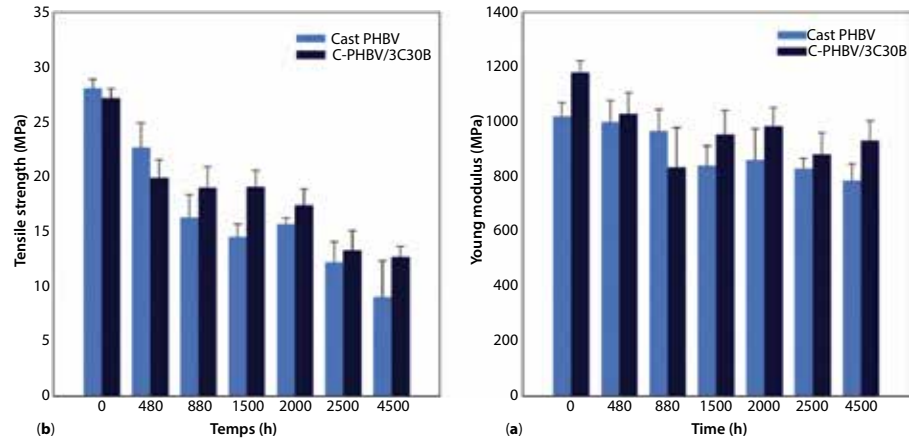


Figure 6 Evolution of (a) Young's modulus, (b) tensile strength for Cast PHBV and C-PHBV/3C30B as a function of exposure time to accelerated photooxidation.

Table 4 Values of Young modulus, tensile strength and elongation at break measured by tensile test of cast PHBV and C-PHBV/3C30B (3 wt.%) bionanocomposites as a function of exposure time to accelerated photooxydation.

Samples	Exposure time (h)	Young modulus (MPa)	Tensile strength (MPa)	Elongation at break (%)
Cast PHBV	0	1020 ± 51	27 ± 1.4	2.9 ± 0.2
	880	967 ± 78	16 ± 2.0	2.5 ± 0.4
	1500	842 ± 71	15 ± 1.1	2.2 ± 0.4
	2000	861 ± 116	16 ± 1.0	2.2 ± 0.2
	2500	831 ± 31	12 ± 1.9	1.9 ± 0.7
	4500	787 ± 60	09 ± 3.3	1.6 ± 0.3
C-PHBV/3C30B	0	1180 ± 42	28 ± 1.3	2.9 ± 0.1
	880	834 ± 145	19 ± 1.9	2.9 ± 0.1
	1500	954 ± 89	19 ± 1.5	2.9 ± 0.7
	2000	984 ± 68	17 ± 1.5	2.3 ± 0.9
	2500	882 ± 79	13 ± 1.8	1.9 ± 0.4
	4500	932 ± 73	12 ± 1	1.9 ± 0.1

tensile strength and elongation at break of irradiated C-PHBV/3C30B bionanocomposite were reduced by 21%, 54% and 34%, compared to those of irradiated cast PHBV, respectively. The incorporation of clays in PHBV thus appears to limit the loss in mechanical properties of PHBV when exposed to UV aging.

3.5 Fracture Surface Analysis

Figure 7a,b shows SEM micrographs of the fractured surface in liquid nitrogen of the Cast PHBV before and after 4500 h of exposure, respectively. From the SEM images of Cast PHBV (Figure 7a), a regular and smooth surface with some particles of boron nitride, i.e., the nucleating agent present in the PHBV matrix,

is observed. After 4500 h of exposure, it is observed in Figure 7b that the fracture surface of the irradiated sample exhibits noticeable damage, as evidenced by a rough surface and the presence of many cavities of different sizes and shapes. For the C-PHBV/3C30B bionanocomposite sample, the SEM micrograph shown in Figure 8a taken before UV exposure, exhibits a regular surface characterized by a homogeneous dispersion of the clay particles in the PHBV matrix. After 4500 h of exposure, the sample displays significant defects on the fracture surface due to photooxidative degradation effect. These defects are primarily responsible for the loss in tensile strength and elongation at break of both Cast PHBV and C-PHBV/3C30B bionanocomposite.

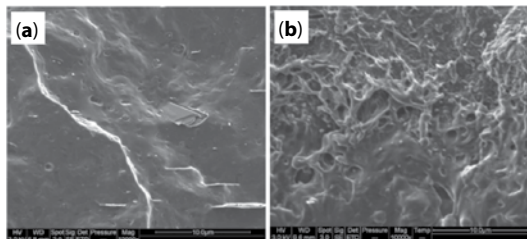


Figure 7 SEM micrographs of fractured surface for Cast PHBV: (a) Before exposure and (b) after 4500 h of accelerated photooxidation exposure.

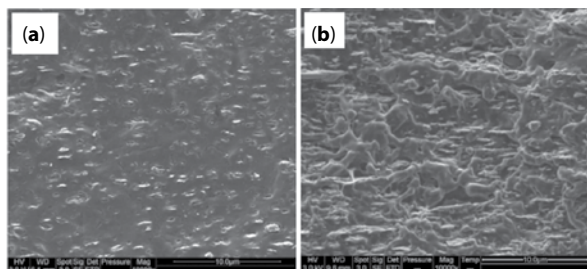


Figure 8 SEM micrographs of fractured surface for C-PHBV/3C30B: (a) Before exposure and (b) after 4500 h of accelerated photooxidation exposure.

4 CONCLUSIONS

In this study, the effect of accelerated photooxidation on the molecular weight and thermal and mechanical properties as well as fracture surfaces of PHBV/Cloisite 30B (3 wt%) bionanocomposite was investigated with respect to Cast PHBV. The data obtained show that photooxidation causes several changes in both the molecular weight and physico-mechanical properties of the irradiated samples, being more pronounced with increasing exposure time. Results indicate that the main degradation mechanism occurring in the accelerated photooxidation of both Cast PHBV and C-PHBV/3C30B bionanocomposites is chain scission, resulting in the decrease of molecular weight. Differential scanning calorimetry (DSC) data indicate a decrease in the degree of crystallinity and melting temperature after UV exposure, with the appearance of double melting peaks, related to the changes in the crystal structure of PHBV. The thermal and mechanical properties are significantly altered for all irradiated samples with exposure time. However, the incorporation of 3 wt% of C30B into the PHBV matrix reduces the degradation rate of bionanocomposite sample. In contrast, thermal stability, tensile strength and elongation at break are significantly decreased for Cast PHBV under accelerated UV testing, whereas these properties are much better for C-PHBV/3C30B bionanocomposite.

This study thus opens up interesting perspectives on the durability of PHA performances in service use when subjected to environmental aging.

REFERENCES

1. S. Bocchini, K. Fukushima, A.D. Blasio, A. Fina, A. Frache, and F. Geobaldo, Poly(lactic acid) and poly(lactic acid)-based nanocomposite photooxidation. *Biomacromol.* **11**(11), 2919–2926 (2010).
2. E. Olewnik-Kruszkowska, I. Koter, J. Skopińska-Wiśniewska, and J. Richert, Degradation of poly(lactide) composites under UV irradiation at 254 nm. *J. Photochem. Photobiol. A* **311**, 144–153 (2015).
3. S. Commereuc, H. Askanian, V. Verney, A. Celli, P. Marchese, and C. Berti, About the end life of novel aliphatic and aliphatic-aromatic (co)polyesters after UV weathering: Structure/degradability relationships. *Polym. Degrad. Stab.* **98**, 1321–1328 (2013).
4. J.K. Pandey, K. Raghunatha Reddy, A. Pratheep Kumar, and R.P. Singh, An overview on the degradability of polymer nanocomposites. *Polym. Degrad. Stab.* **88**, 234–250 (2005).
5. S. Slater, D. Glassner, E. Vink, and T. Gerngross, Evaluating the environmental impact of biopolymers in biopolymers, in *Biopolymers Online*, A. Steinbüchel (Ed.), vol. 10, pp. 474–491 (2006).
6. N. Pons, A. Bergeret, J.-C. Benezet, L. Ferry, and F. Fesquet, An environmental stress cracking (ESC) test to study the ageing of biopolymers and biocomposites. *Polym. Test.* **30**, 310–317 (2011).
7. M. Day, K. Shaw, D. Cooney, J. Watts, and B. Harrigan, Degradable polymers: The role of the degradation environment. *J. Environ. Polym. Degrad.* **5**(3), 137–151 (1997).
8. S.M. Halliwell and D. Gardiner, Artificial weathering procedures for plastics glazing materials. *Constr. Build. Mater.* **8**(4), 233–241 (1994).
9. K. Fukushima, D. Tabuani, C. Abbate, M. Arena, and P. Rizzarelli, Preparation, characterization and biodegradation of biopolymer nanocomposites based on fumed silica. *Eur. Polym. J.* **47**, 139–152 (2011).
10. K. Fukushima, D. Tabuani, C. Abbate, M. Arena, and L. Ferreri, Effect of sepiolite on the biodegradation of poly(lactic acid) and polycaprolactone. *Polym. Degrad. Stab.* **95**, 2049–2056 (2010).
11. E. Bugnicourt, P. Cinelli, A. Lazzeri, and V. Alvarez, Poly(hydroxyalkanoate) (PHA): review of synthesis, characteristics, processing and potential applications in packaging. *Express Polym. Lett.* **8**, 791–808 (2014).
12. L. Wei, N.M. Guho, E.R. Coats, and A.G. McDonald, Characterization of poly(3-hydroxybutyrate-co-3-hydroxyvalerate) biosynthesized by mixed microbial consortia fed fermented dairy manure. *J. Appl. Polym. Sci.* **131**, 40333 (2014).
13. A. Gonzalez, L. Irusta, M.J. Fernández-Berridi, M. Iriarte, and J.J. Iruin, Application of pyrolysis/gas chromatography/Fourier transform infrared spectroscopy and TGA techniques in the study of thermal degradation

- of poly(3-hydroxybutyrate). *Polym. Degrad. Stab.* **87**(2), 347–354 (2005).
14. H. Ariffin, H. Nishida, Y. Shirai, and M.A. Hassan, Determination of multiple thermal degradation mechanisms of poly(3-hydroxybutyrate). *Polym. Degrad. Stab.* **93**(8), 1433–1439 (2008).
 15. H. Tsuji, and K. Suzuyoshi, Environmental degradation of biodegradable polyesters 1. Poly(ϵ -caprolactone), poly[(R)-3-hydroxybutyrate], and poly(L-lactide) films in controlled static seawater. *Polym. Degrad. Stab.* **75**, 347–355 (2002).
 16. D.S. Rosa, M.R. Calil, C.G.F. Guedes, and T.C. Rodrigues, Biodegradability of thermally Aged PHB, PHB-V, and PCL in soil compostage. *J. Polym. Environ.* **12**, 239–245 (2004).
 17. M.N. Kim, A.R. Lee, J.S. Yoon, and I.J. Chin, Biodegradation of poly(3-hydroxybutyrate), Sky-Green® and Mater-Bi® by fungi isolated from soils. *Eur. Polym. J.* **36**, 1677–1685 (2000).
 18. L. Wei, S. Liang, and A.G. McDonald, Thermophysical properties and biodegradation behavior of green composites made from polyhydroxybutyrate and potato peel waste fermentation residue. *Ind. Crop. Prod.* **69**, 91–103 (2015).
 19. C. Eldsater, S. Karlsson, and A.C. Albertsson, Effect of abiotic factors on the degradation of poly(3-hydroxybutyrate-co-3-hydroxyvalerate) in simulated and natural composting environments. *Polym. Degrad. Stab.* **64**, 177–183 (1999).
 20. K. Iggui, N. Le Moigne, S. Cambe, J.R. Degorce-Dumas, M. Kaci, and A. Bergeret, A biodegradation study of poly(3-hydroxybutyrate-co-3-hydroxyvalerate) / organo-clay nanocomposites in various environmental conditions. *Polym. Degrad. Stab.* **119**, 77–86 (2015).
 21. T. Iwata, Y. Doi, K. Kasuya, and Y. Inoue, Visualization of enzymatic degradation of poly[(R)-3 hydroxybutyrate] single crystals by an extracellular PHB depolymerase. *Macromol.* **30**, 833–839 (1997).
 22. T. Iwata, Y. Doi, T. Tanaka, T. Akehata, M. Shiromo, and S. Teramachi, Enzymatic degradation and adsorption on poly[(R)-3-hydroxybutyrate] single crystals with two types of extracellular PHB depolymerases from *Comamonas acidovorans* YM1609 and *Alcaligenes faecalis* T1. *Macromol.* **30**, 5290–5296 (1997).
 23. L. Wei and A.G. McDonald, Accelerated weathering studies on the bioplastic, poly(3 hydroxybutyrate-co-3-hydroxyvalerate). *Polym. Degrad. Stab.* **126**, 93–100 (2016).
 24. R.K. Sadi, G.J.M. Fehine, and N.R. Demarquette, Photodegradation of poly(3-hydroxybutyrate). *Polym. Degrad. Stab.* **95**, 2318–2327 (2010).
 25. A.T. Michel and S.L. Billington, Characterization of poly-hydroxybutyrate films and hemp fiber reinforced composites exposed to accelerated weathering. *Polym. Degrad. Stab.* **97**, 870–878 (2012).
 26. M.A. Paul, C. Delcourt, M. Alexandre, P. Degée, F. Monteverde, and P. Dubois, Poly-lactide/montmorillonite nanocomposites: Study of the hydrolytic degradation. *Polym. Degrad. Stab.* **87**(3), 535–542 (2005).
 27. S. Ray, K. Yamada, M. Okamoto, and K. Ueda, Control of biodegradability of poly-lactide via nanocomposite technology. *Macromol. Mat. Eng.* **288**(4), 203–208 (2003).
 28. J.A. Ratto, D.M. Steeves, E.A. Welsh, and B.E. Powell, A study of polymer/clay nanocomposites for biodegradable applications. *Proc. SPE Ann. Tech. Conf.* **45**, 1628–1632 (1999).
 29. P. Maiti, A. Batt Carl, and E.P. Giannelis, New biodegradable polyhydroxybutyrate/layered silicate nanocomposites. *Biomacromol.* **8**, 3393–3400 (2007).
 30. P. Bordes, E. Pollet, and L. Avérous, Nano-biocomposites: Biodegradable polyester/nanoclay systems. *Prog. Polym. Sci.* **34**, 125–155 (2009).
 31. P. Bordes, E. Hablot, E. Pollet, and L. Avérous, Effect of clay organomodifiers on degradation of polyhydroxyalkanoates. *Polym. Degrad. Stab.* **94**, 789–796 (2009).
 32. E. Hablot, P. Bordes, E. Pollet, and L. Avérous, Thermal and thermo-mechanical degradation of poly(3-hydroxybutyrate)-based multiphase systems. *Polym. Degrad. Stab.* **93**, 413–421 (2008).
 33. T. Wu and C. Wu, Biodegradable poly(lactic acid)/chitosan-modified montmorillonite nanocomposites: Preparation and characterization. *Polym. Degrad. Stab.* **91**(9), 2198–2204 (2006).
 34. K. Wu, C. Wu, and J. Chang, Biodegradability and mechanical properties of polycaprolactone composites encapsulating phosphate-solubilizing bacterium *Bacillus* sp. PG01. *Process. Biochem.* **42**(4), 669–675 (2007).
 35. Y. Someya, N. Kondo, and M. Shibata, Biodegradation of poly(butylene adipate-co-butylene terephthalate)/layered-silicate nanocomposites. *J Appl. Polym. Sci.* **106**(2), 730–736 (2007).
 36. P.J. Barham, A. Keller, E.L. Otun, and P.A. Holmes, Crystallization and morphology of a bacterial thermoplastic: Poly-3-hydroxybutyrate. *J. Mater. Sci.* **19**, 2781–2794 (1984).
 37. L. Zaidi, S. Bruzaud, M. Kaci, A. Bourmaud, N. Gautier, and Y. Grohens, The effects of gamma irradiation on the morphology and properties of polylactide/Cloisite 30B nanocomposites. *Polym. Degrad. Stab.* **98**, 348–355 (2012).
 38. L. Zaidi, M. Kaci, S. Bruzaud, A. Bourmaud, and Y. Grohens, Effect of natural weather on the structure and properties of polylactide/Cloisite 30B nanocomposites. *Polym. Degrad. Stab.* **95**, 1751–1758 (2010).
 39. D.F. Parra, D.S. Rosa, J. Rezende, P. Ponce, and A.B. Lugao, Biodegradation of γ irradiation poly 3-hydroxybutyrate (PHB) films blended with poly(ethyleneglycol). *J. Polym. Environ.* **19**, 918–925 (2014).
 40. L.M. Oliveira, E.S. Araujo, and S.M.L. Guedes, Gamma irradiation effects on poly(hydroxybutyrate). *Polym. Degrad. Stab.* **91**, 2157–2162 (2006).
 41. E.B. Hermida, V.I. Mega, O. Yashchuk, V. Fernandez, P. Eisenberg, and S.S. Miyazaki, Gamma irradiation effects on mechanical and thermal properties and biodegradation of poly(3-hydroxybutyrate) based films. *Macromol. Symp.* **263**, 102–113 (2008).
 42. H. Mitomo, Y. Watanabe, I. Ishigaki, and T. Saito, Radiation-induced degradation of poly(3-hydroxybutyrate) and

- the copolymer poly(3-hydroxybutyrate-co-3-hydroxyvalerate). *Polym. Degrad. Stab.* **45**, 11–17 (1994).
43. A. Bergmann, J. Tebmar, and A. Owen, Influence of electron irradiation on the crystallisation, molecular weight and mechanical properties of poly-(R)-3-hydroxybutyrate. *J. Mater. Sci.* **42**, 3732–3738 (2007).
 44. Y. Zhang, J. Xu, and B. Guo, Photodegradation behavior of poly(butylene succinate-co-butylene adipate)/ZnO nanocomposites. *Colloids Surf. A: Physicochem. Eng. Asp.* **489**, 173–181 (2016).
 45. M. Yasuniwa, S. Tsubakihara, Y. Sugimoto, and C. Nakafuku, Thermal analysis of the double-melting behavior of poly(L-lactic acid). *J. Polym. Sci. B Polym. Phys.* **42**, 25–32 (2004).
 46. S. Solarski, M. Ferreira, and E. Devaux, Ageing of polylactide and polylactide nanocomposite filaments. *Polym. Degrad. Stab.* **93**, 707–713 (2008).
 47. M.S. Islam, K.L. Pickering, and N.J. Foreman, Influence of accelerated ageing on the physico-mechanical properties of alkali-treated industrial hemp fibre reinforced poly(lactic acid) (PLA) composites. *Polym. Degrad. Stab.* **95**, 59–65 (2010).
 48. G. Gorrasi, C. Milone, E. Piperopoulos, M. Lanza, and A. Sorrentino, Hybrid clay mineral-carbon nanotube-PLA nanocomposite films. Preparation and photodegradation effect on their mechanical, thermal and electrical properties. *Appl. Clay Sci.* **71**, 49–54 (2013).